Int. J. Heat Mass Transfer. Vol. 32, No. 2, pp. 201–212, 1989
Printed in Great Britain

0017–9310/89 $3.00 + 0.00

Heat transfer in a straight tube situated downstream of a bend

M. M. OHADI† and E. M. SPARROW
Department of Mechanical Engineering, University of Minnesota, Minneapolis, MN 55455, U.S.A.

(*Received* 6 *April* 1988 *and in final form* 15 *July* 1988)

Abstract—The axial variation of the local heat transfer coefficient in a straight tube situated downstream of a bend is measured by a mass transfer technique for parametric values of the Reynolds number (5000–85 000), bend turn angle (0, 30, 60, and 90°), and flow condition at the bend inlet. For one flow condition, the bend inlet is fed by a hydrodynamically developed tube flow. In a second case, the bend is fed from a large upstream plenum through a sharp-edged inlet. The Schmidt number for the mass transfer is 2.5 (naphthalene sublimation in air). It is found that the presence of a bend fed from a plenum through a sharp-edged inlet gives rise to a decrease in the mass (heat) transfer coefficients in the downstream tube compared with those for the no-bend case. On the other hand, a bend fed with a developed flow generally tends to decrease the coefficients in the downstream tube at lower Reynolds numbers while increasing the coefficients at higher Reynolds numbers. For both bend inlet configurations, there is clear evidence of laminarization of the flow at the lower Reynolds numbers and larger bend turn angles.

INTRODUCTION

THIS PAPER reports an experimental study of forced convection heat transfer in a circular tube the inlet of which is situated immediately downstream of a bend. The tube is, therefore, the recipient of the velocity distribution which exits the bend. As will be discussed shortly, the velocity distribution presented to the tube by the bend is highly complex and is significantly different from those normally encountered in circular tubes. Once the bend-presented velocity distribution enters the tube, it undergoes a redevelopment such that at sufficiently great downstream distances, a conventional fully developed pipe flow is attained.

In the bend, the curvature of the flow induces a cross-sectional pressure variation such that the pressure increases in the direction away from the center of curvature of the bend. As a result of the pressure variation, the slow-moving fluid adjacent to the wall moves toward the center of curvature while, to satisfy continuity, the faster-moving fluid in the core moves away from the center of curvature. In this way, two symmetrically placed, counter-rotating eddies are established in the cross section of the bend. The superposition of these eddies on the streamwise mainflow gives rise to helical motions within each eddy.

The specifics of the flow field at the exit of the bend depend on the streamwise length of the bend since, as in a straight pipe, hydrodynamic development is a progressive process and requires sufficient length for completion. Furthermore, if hydrodynamic development is not complete at the bend exit, the specifics of the bend exit flow will depend on the bend inlet conditions. The influence of the length of the bend (i.e. the turn angle of the bend) and the bend inlet conditions will be addressed in the present research. These factors were found to have a significant effect on the heat transfer characteristics of the bend itself [1].

The foregoing discussion sets the stage for the present investigation in that it establishes the special nature of the velocity field in a tube situated downstream of a bend. On this basis, there is ample justification to expect that the forced convection heat transfer characteristics of such a tube will differ significantly from those of a conventional pipe flow.

A schematic view of the physical situations to be studied here is presented in Figs. 1 and 2. The distinction between the two figures is that they display configurations which yield different conditions at the *bend inlet*.

In Fig. 1, a length of a straight circular tube designated as the mass transfer section is situated downstream of a bend which, in turn, is fed by another length of straight tube termed the development section. The presence of the mass transfer section reflects the fact that mass transfer measurements, coupled with the analogy between heat and mass, were performed to obtain heat transfer results. The mass transfer measurements yielded streamwise distributions of the axially quasi-local, circumferential-average mass transfer coefficient. The mass transfer section was of length L and internal diameter D, with local axial positions being identified by the coordinate X measured from the onset of mass transfer.

The bend geometry was defined by the turn angle

† Present address: Department of Mechanical Engineering, Michigan Technological University, Houghton, MI 49931, U.S.A.

NOMENCLATURE

A	mass transfer surface area
D	internal diameter
D_B	diameter of baffle plate
$\mathscr{D}$	diffusion coefficient
K	mass transfer coefficient, equation (2)
L	length of mass transfer section
L_H	length of hydrodynamic development tube
ΔM	change of mass
$\dot{m}$	rate of mass transfer per unit area
$\dot{Q}$	volumetric flow rate
R	internal radius of bend
R_c	radius of curvature of bend centerline
Re	Reynolds number, $4\dot{w}/\mu\pi D$
Sc	Schmidt number
Sh	Sherwood number, $KD/\mathscr{D}$
$\dot{w}$	mass flow rate
X	axial coordinate in mass transfer section.

Greek symbols

θ	bend turn angle
μ	viscosity
ν	kinematic viscosity
ρ_{nb}	naphthalene vapor density in bulk
ρ_{nw}	naphthalene vapor density at wall
τ	duration of data run.

Subscript

i	mass transfer element i.

θ, the radius of curvature R_c of the bend centerline, and the radius R ($= D/2$) of the bend cross section. The straight tube which fed the bend was employed with a view to providing hydrodynamically developed flow at the bend inlet, and its L_H/D ratio was chosen accordingly (L_H and D are, respectively, the length and diameter of the hydrodynamic development section). As indicated by the measured linearity of the axial pressure distribution, hydrodynamic development was completed well upstream of the bend inlet. However, the upstream propagation of the pressure field in the bend [2] gave rise to small deviations from the developed state at the bend inlet.

All components along the path of the fluid flow shared the same internal diameter D. The development tube was tangent to the upstream end of the bend, and the mass transfer tube was tangent to the downstream end of the bend. Neither the bend, the development tube, nor any piping downstream of the mass transfer tube participated in the mass transfer process. In terms of the analogous heat transfer situation, these components were adiabatic. With regard to the mass transfer section, the analogous thermal boundary condition is uniform wall temperature.

Attention may now be turned to Fig. 2. The setup shown in Fig. 2 differs from that of Fig. 1 in that the hydrodynamic development tube which fed the bend is now absent, exposing the bend inlet to the laboratory. To better define the inlet conditions, the bend inlet was framed by a large circular baffle plate (diameter D_B). With the baffle in place, air was drawn into the bend inlet only from the space upstream of the inlet, so that the laboratory served as a large plenum chamber with the baffle as its downstream wall. The geometry of the inlet was carefully machined to give a sharp edge. As is well known, this type of inlet gives rise to flow separation, the ramifications of which will be evident later. As was true for the setup of Fig. 1, only the mass transfer section in Fig. 2 participated in the mass transfer process.

The experiments were performed as a function of three parameters: (1) the pipe-flow Reynolds number Re, which ranged from about 5000 to 85 000, (2) the turn angle θ of the bend, the values of which were 0, 30, 60, and 90°, and (3) the bend inlet configuration—either tube fed or sharp edged. The Reynolds number range spans the low to fully turbulent regimes for pipe flows although, as will be seen later, the presence of the bend promotes laminarization at the lower Reynolds numbers. The $\theta = 0°$ case corresponds to the absence of the bend, so that this case can serve as a baseline against which the other cases can be compared.

Aside from the aforementioned, the other relevant parameters were held fixed. These include the Schmidt number for the mass transfer process (naphthalene sublimation in air), the value of which is 2.5. Also, the bend curvature was characterized by $R_c/R = 9$. Other geometrical parameters, the values of which

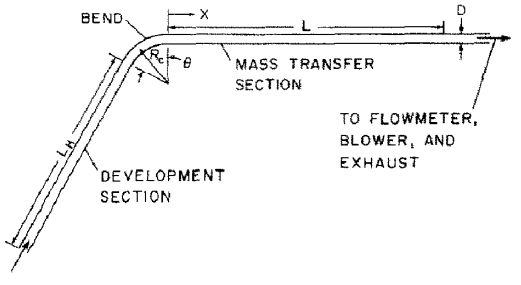

FIG. 1. Mass transfer section downstream of a bend with a tube-fed inlet.

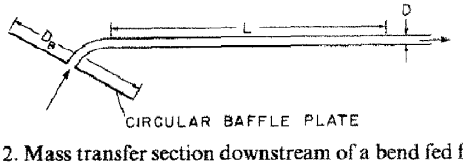

FIG. 2. Mass transfer section downstream of a bend fed from a large upstream plenum through a sharp-edged inlet.

are less critical, include $L/D = 20.4$, $L_H/D = 30$, and $D_B/D = 16$.

For each Re, θ, and bend inlet configuration, the local Sherwood number (dimensionless mass transfer coefficient) was determined at 21 axial stations along the length of the mass transfer section. The thus-determined axial distributions will be presented in formats chosen to highlight the parametric dependencies.

The reference list for the present paper is necessarily short because the authors were unable to find any prior information on heat or mass transfer in tubes situated downstream of bends. With regard to the bend-induced laminarization mentioned in the foregoing, the relevant references are to Taylor [3] and to Narasimha and Sreenivasan [4], which will be elaborated later. A general review of fluid flow in bends is available in ref. [5].

EXPERIMENTAL APPARATUS AND PROCEDURE

The heart of the experimental apparatus, the mass transfer section, was a circular tube made up of a linear assembly of 21 individual mass transfer elements. Each element was a composite annular cylinder, with an external metallic cylindrical shell and an annular core of naphthalene. The inner surface of the naphthalene served to bound the flow passage. This surface was hydrodynamically smooth, having been cast against a highly polished and lapped brass shaft. The casting procedure, which is described in ref. [6], produced a uniform diameter flow passage with $D = 3.175$ cm $= 1.250$ in. Mass transfer occurred due to the sublimation of the naphthalene into the airflow in the passage.

The successive mass transfer elements were mated by means of interlocking tongues and recesses which had been machined into the metallic cylindrical shells at their downstream and upstream ends. The interlocking of the elements is similar to that shown in Fig. 1 of ref. [7], except that the present elements had longer tongues and recesses than those of ref. [7] in order to ensure more exact axial straightness of the assembly. The attainment of straightness was further aided by an adjustable support situated beneath the assembled tube.

Once the elements had been assembled, the assembly was made into a single unit by a sustained force applied by means of quick-acting, self-locking clamps. Potential leakage at the interfaces of successive elements was totally eliminated (as verified by pressurization tests) by highly adhesive tape which bridged across the interfaces at the exterior surface of the metallic shells.

In recognition of the expected more rapid variations of the mass transfer coefficient near the tube inlet and the less rapid variations further downstream, mass transfer elements of different axial length were employed to obtain highly accurate quasi-local transfer coefficients. To this end, shorter elements were used at the upstream end of the tube and longer elements downstream. The lengths of the respective mass transfer surfaces of elements 1–7 were $0.4D$, those of elements 8–13 were $0.8D$, and those of elements 14–21 were $1.6D$. Thus, the overall axial length of the mass transfer surface of the assembled tube was $20.4D$.

To facilitate the data reduction, which requires the density of naphthalene vapor at the subliming surface, two of the elements, 1 and 21, were equipped with fine-gage, precalibrated thermocouples. The thermocouples were cast in place in the naphthalene such that the junctions were positioned at the bounding surface of the flow passage.

The bends used in the present experiments had been fabricated earlier in connection with a study of axial and circumferential pressure distributions in bends [2]. Three bends were available, with respective turn angles $\theta = 30$, 60, and 90°. All bends had a cross-sectional diameter $D = 3.175$ cm (1.250 in.), identical to that of the mass transfer section. Also, all bends had the same centerline radius of curvature $R_c = 14.29$ cm (5.625 in.), resulting in an R_c/R ratio of 9.

As noted earlier, in one of the two investigated bend inlet configurations, the bend was fed with airflow delivered to it by a hydrodynamic development tube. The tube was 3.175 cm (1.250 in.) in internal diameter and 30 diameters in length. It was equipped with a linear array of pressure taps deployed along its length. At the two instrumented stations nearest the bend (namely, $0.5D$ and $1D$), there were three taps distributed around the circumference. The pressure taps were installed to detect the attainment of hydrodynamically developed flow (linear axial pressure variation) and any precursive effects due to the presence of the bend (i.e. circumferential pressure variations upstream of the bend). The upstream end of the development tube was open to the laboratory and presented a sharp-edged inlet to the airflow.

The other investigated bend inlet condition is the sharp-edged inlet, and the rationale for using a baffle plate to more precisely define this condition has already been discussed. The baffle plate was a circular aluminum disk, 50.8 cm (20 in.) in diameter and 0.318 cm (0.125 in.) thick. However, its thickness was reduced to 0.127 cm (0.050 in.) where the baffle framed the bend inlet, thereby adding an upstream extension of only $0.04D$ to the bend. For the $\theta = 0°$ turn angle (no bend), the thickness was further reduced so that the resulting non-mass-transfer-participating upstream extension of the mass transfer section was only $0.02D$. These unintended extensions are not expected to have any effect on the results.

Downstream of the mass transfer section, the piping system continued the section's 3.175 cm (1.250 in.) internal diameter for a length of about 12 diameters. Thereafter, the piping was enlarged to a diameter appropriate to the rotameters used for measurement of the mass flow rate. Various rotameters were used

depending on the magnitude of the flow. After the rotameter, the flow passed through a control valve and was then ducted to a blower. The blower was situated in a service corridor adjacent to the laboratory, and the compression-heated, naphthalene-enriched discharge from the blower was vented outside the building.

The downstream positioning of the blower meant that the apparatus was operated in the suction mode, with air drawn into the apparatus from the laboratory. Since the laboratory was temperature controlled and free of naphthalene vapor, the condition of the air entering the apparatus was thus well established. The entering air temperature was measured by a thermocouple positioned just upstream of the inlet.

The execution of a data run involved a number of steps which required considerable care and attention to detail. The preparation of the mass transfer elements via a casting procedure was the starting point. Once cast, the elements were placed in a sealed container and allowed to equilibrate to achieve temperature equality with the laboratory. Then, the mass transfer section was assembled for a brief pre-run to allow further thermal equilibration, alignment of the assembly for axial straightness, removal of naphthalene dust or chips, and fine tuning of the setting of the control valve.

After the pre-run, the mass transfer section was disassembled and each element was carefully weighed on an ultraprecision analytical balance (resolution of 0.00001 g). Upon completion of the weighing, the elements were reassembled and the apparatus was put into final form for the data run. The duration of the run (i.e. duration of the airflow period) was selected such that the average change in the diameter of any element due to sublimation did not exceed 0.0025 cm (0.001 in.). For example, for the case of the tube-fed inlet, duration times ranged from 7 to 55 min for Reynolds numbers in the range from about 84000 to 5000. During a run, data were collected for the temperatures at the mass transfer elements and in the ambient, for the rotameter and barometric pressures, and for the indicated rotameter flow rates.

At the conclusion of the run, the mass transfer section was disassembled and the individual elements weighed. After the post-run weighing, a procedure was performed to determine a correction for any extraneous mass transfer which might have occurred during the periods of assembly, disassembly, and weighing. This procedure involved repeating all the steps of the actual data run, but with the airflow period omitted. The procedure terminated with a final weighing of the elements. On the average, the correction for extraneous losses was about 2.5% of the mass transfer during the data run proper.

DATA REDUCTION

The main objective of the data reduction was to evaluate the mass transfer coefficient and Sherwood number at each element of the mass transfer section for each data run and also to evaluate the Reynolds number for each run. Since the measured mass transfer rate for each element corresponds to the element as a whole, the resulting transfer coefficient and Sherwood number are circumferential and axial averages. However, since the lengths of the elements were chosen to be short relative to the prevailing axial variations, the per-element results may be regarded as being axially quasi-local. In the forthcoming presentation of results, the Sherwood number for each element will be plotted at an axial coordinate which corresponds to the axial midpoint of the element.

For the data reduction, the successive elements will be numbered $1, 2, \ldots, 21$, with i being a typical element. For element i, the mass transferred during a data run of duration τ will be denoted by ΔM_i, where ΔM_i includes a correction for extraneous mass losses determined as described earlier. The surface area for mass transfer from element i is A_i. In determining A_i, account was taken of the slight change in the diameter of the flow passage which occurs due to sublimation during the data run. With these quantities, the per-element mass transfer per unit time and unit area is

$$\dot{m}_i = \Delta M_i/\tau A_i. \tag{1}$$

The mass transfer at each element is driven by the difference between the densities of the naphthalene vapor at the wall and in the bulk, respectively, $\rho_{\mathrm{nw},i}$ and $\rho_{\mathrm{nb},i}$. Under the assumption that solid–vapor equilibrium prevails at the wall, ρ_{nw} is a function of temperature, and since the temperature is uniform along the wall (by measurement), so is ρ_{nw}. Therefore, $\rho_{\mathrm{nw},i} = \rho_{\mathrm{nw}}$. On the other hand, ρ_{nb} increases along the length of the mass transfer section, so that subscript i must be retained for ρ_{nb}.

In terms of the foregoing quantities, the mass transfer coefficient for element i follows as

$$K_i = \dot{m}_i/(\rho_{\mathrm{nw}} - \rho_{\mathrm{nb},i}). \tag{2}$$

The value of ρ_{nw} was found by introducing the measured wall temperature into the vapor pressure–temperature relation for naphthalene [8] and then substituting the vapor pressure into the perfect gas law.

For the determination of $\rho_{\mathrm{nb},i}$, it is first relevant to note that the rise of ρ_{nb} experienced by the airflow passing through any element j is

$$(\Delta\rho_{\mathrm{nb}})_j = (\Delta M_j/\tau)/\dot{Q} \tag{3}$$

where $\dot{Q}$ is the volumetric flow rate. Consequently, the values of ρ_{nb} at the inlet and exit cross sections of element i are

$$\sum_{j=1}^{i-1} (\Delta M_j/\tau)/\dot{Q}, \qquad \sum_{j=1}^{i} (\Delta M_j/\tau)/\dot{Q} \tag{4}$$

and $\rho_{\mathrm{nb},i}$ will be taken as the average of these, so that

$$\rho_{\mathrm{nb},i} = \sum_{j=1}^{i-1} (\Delta M_j/\tau)/\dot{Q} + 0.5(\Delta M_i/\tau)\dot{Q}. \tag{5}$$

In both equations (4) and (5), it is assumed that $\rho_{nb} = 0$ at the beginning of the mass transfer section, a condition fulfilled by the suction-mode operation and the absence of naphthalene vapor in the laboratory. It was also assumed that $\dot{Q}$ is constant along the length of the mass transfer section, a condition which was satisfactorily fulfilled for all the experiments.

Once K_i has been determined, the per-element Sherwood number is evaluated from its definition

$$Sh_i = K_i D/\mathscr{D} \tag{6}$$

where $\mathscr{D}$ is the mass diffusion coefficient. This quantity can be eliminated by introducing the Schmidt number $Sc = \nu/\mathscr{D}$, so that

$$Sh_i = (K_i D/\nu)Sc. \tag{7}$$

For naphthalene–air mixtures, $Sc = 2.5$ [8]. The kinematic viscosity ν was taken as that for pure air since the concentrations of naphthalene vapor were minute.

For the Reynolds number, the standard processing of the volumetric flow rate indicated by the rotameter yielded the mass flow rate $\dot{w}$. Then

$$Re = 4\dot{w}/\mu\pi D \tag{8}$$

where μ was evaluated for pure air.

RESULTS AND DISCUSSION

Before presenting the results of the present experiments, it is relevant to provide collateral information which serves to establish the accuracy of the data. Such an accuracy assessment has to be based on the no-bend case, since there appears to be no prior information on heat or mass transfer in a straight tube downstream of a bend.

Fully developed Sherwood numbers for the no-bend case, as measured in the present apparatus, are compared with the widely-accepted correlations of Petukhov–Popov and of Gnielinski for turbulent pipe flow in Fig. 4 of ref. [9]. Truly excellent agreement of the data with the correlations was found to prevail. For turbulent heat or mass transfer in a tube fed by a hydrodynamic development length, it is possible to compute the transfer coefficients in the thermal or mass entrance region. Such computations were performed in ref. [10] and compared (in Fig. 4 of ref. [10]) with the entrance region mass transfer coefficients measured with the present apparatus. Excellent agreement between the numerical predictions and the data prevailed throughout the entire entrance region. The just-cited comparisons provide a high degree of confidence in the accuracy of the data obtained from the present experiments.

The focus of the presentation will now be directed to the bend-related effects on the Sherwood numbers downstream of the bend. The first set of results corresponds to bends the inlets of which are fed by a hydrodynamic development tube, while the second set of results corresponds to bends which have a sharp-edged inlet. Finally, the results for the two bend inlet configurations are brought together and compared.

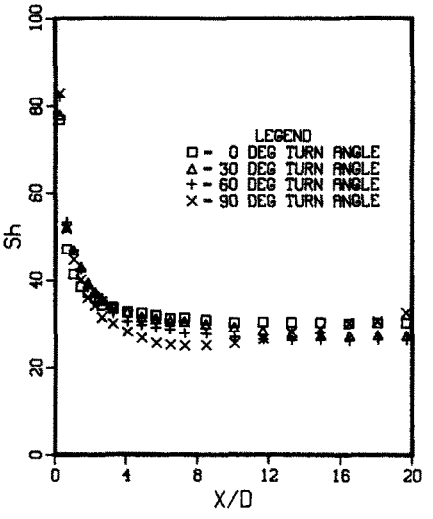

FIG. 3. Sherwood number distributions in the mass transfer section downstream of a bend with a tube-fed inlet, $Re \cong 5450$.

Tube-fed bend inlet

The Sherwood number distributions in the mass transfer section downstream of the bend are presented in Figs. 3–8 for the case of the tube-fed bend inlet. In each figure, which corresponds to a given Reynolds number, the axially quasi-local Sherwood number is plotted as a function of the dimensionless axial distance X/D downstream of the onset of mass transfer. (Note that $X = 0$ also corresponds to the beginning of the straight tube which follows the bend.) As noted earlier, the measured Sherwood number for each mass

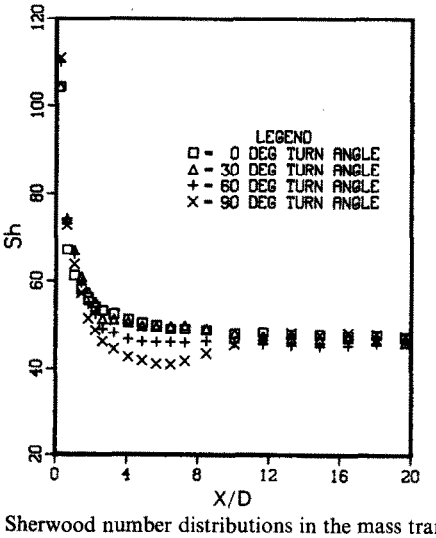

FIG. 4. Sherwood number distributions in the mass transfer section downstream of a bend with a tube-fed inlet, $Re \cong 9090$.

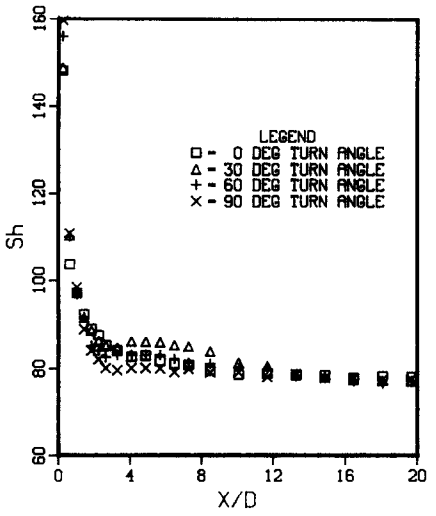

FIG. 5. Sherwood number distributions in the mass transfer section downstream of a bend with a tube-fed inlet, $Re \cong 15\,800$.

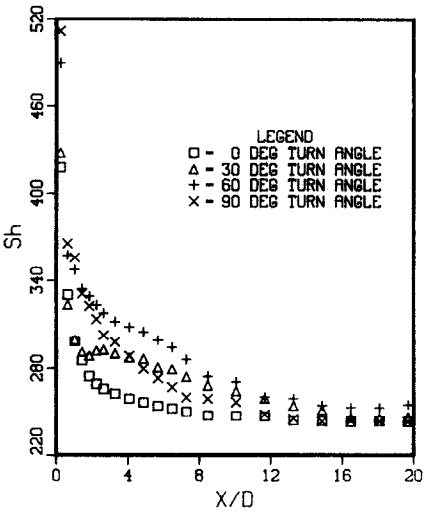

FIG. 7. Sherwood number distributions in the mass transfer section downstream of a bend with a tube-fed inlet, $Re \cong 60\,800$.

transfer element is plotted at the X coordinate which corresponds to the axial midpoint of the element.

In each figure, data are presented for four bend turn angles: 0 (no bend), 30, 60, and 90°. This format, whereby the turn angle is the curve parameter, was chosen to provide easy identification of the effect of the presence of the bend, with the no-bend case serving as a baseline. The Reynolds numbers for the four turn angles appearing in each figure are not quite the same, and the figure is labeled with the average value. For most of the figures, the overall spread in the Reynolds number is in the 1% range, with overall spreads of 2.9 and 2.1 in Figs. 3 and 7. These spreads should not materially affect the comparisons of the results for the various turn angles.

All of the figures have a common abscissa scale which ranges from $X/D = 0$ to 20. However, the ordinate scale of each figure is tailored to accommodate the Sherwood number range appropriate to each of the investigated Reynolds numbers. Because of the different scales and because all scales are linear, the data scatter, which is generally about 2%, is portrayed somewhat differently in the various figures.

The first objective of an overall inspection of Figs. 3–8 is to identify broad generalizations. The broadest and most useful generalization would be that the presence of a bend gives rise to either a consistent increase or a consistent decrease in the Sherwood numbers relative to those for the no-bend case. However, neither of these characterizations is generally applicable to the comparison of the with-bend and no-bend results conveyed in Figs. 3–8. The absence of a broad

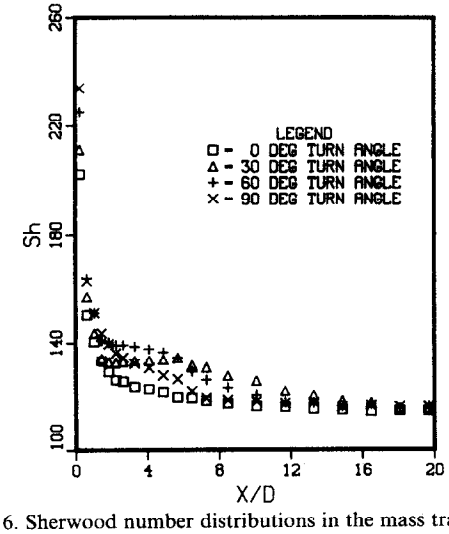

FIG. 6. Sherwood number distributions in the mass transfer section downstream of a bend with a tube-fed inlet, $Re \cong 24\,500$.

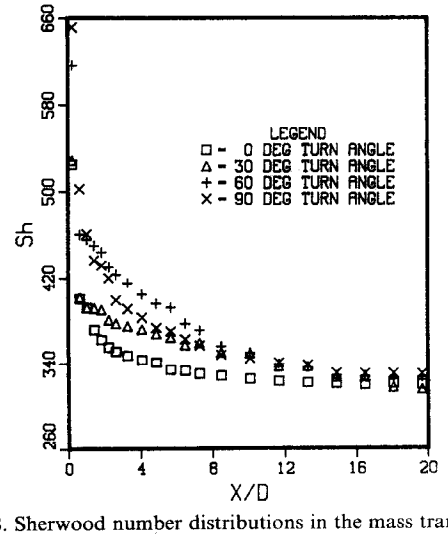

FIG. 8. Sherwood number distributions in the mass transfer section downstream of a bend with a tube-fed inlet, $Re \cong 83\,000$.

generalization necessitates a more detailed discussion of the results, as follows.

The mass transfer section downstream of the bend is, at least in its initial portion, a mass transfer entrance region. The Sherwood number distribution in a conventional entrance region with an axially unchanging, fully developed velocity profile is very well exemplified by those for the no-bend case (i.e. $\theta = 0°$) in Figs. 3–8. Starting with relatively high values at the onset of mass transfer, the Sherwood number decreases monotonically and smoothly to a fully developed value depending on the Reynolds number, with the decrease being rapid at first and more gradual later. In the presence of a bend upstream of the tube, various departures in the shape of the Sherwood number distribution from the aforementioned standard shape are in evidence in the figures.

The most remarkable departure is that for the 90°-bend case in Figs. 3 and 4 ($Re = 5450$ and 9090, respectively). In these cases, the Sherwood number distribution decreased to a minimum at about $X/D = 6$ and, thereafter, increased toward its fully developed value (which is not quite achieved in Fig. 3). Thus, the Sherwood number distribution displays undershoot. The undershoot, relative to the fully developed value, is about 27% for $Re = 5450$ and 22% for $Re = 9090$.

The cause of the undershoot is the laminarization of the flow and the subsequent transition to turbulence. As was demonstrated in refs. [3, 4], a turbulent flow entering a coiled tube may be laminarized. The laminarization occurred after a sufficiently long run in the coiled tube. Since the 90° turn angle provides the longest run of curved flow considered here, it presents the most likely case for laminarization. Also, the likelihood of laminarization is greater at lower Reynolds numbers (e.g. 5450 and 9090).

Careful study of Figs. 3 and 4 suggests that laminarization begun in the bend must have continued in the straight mass transfer section downstream of the bend. This is because there are no evident effects of laminarization at the first data station, i.e. the value of Sh corresponding to the 90° turn angle is higher than the others. Only at larger X/D do the values of Sh for the 90° turn dip low. Once the laminarized (or partially laminarized) flow has moved sufficiently downstream in the tube, it undergoes a transition to turbulence. The transition is responsible for the increase in the Sherwood number after the minimum.

Aside from the just-discussed undershoot for the 90° turn angle, the low Reynolds number (5450, 9090) Sherwood number distributions for the other turn angles follow the conventional pattern. However, as the Reynolds number increases, other unconventional features appear in the distributions. For the 30° turn, for $Re = 15\,800$, 24 500, and 60 800, the initial sharp decrease in Sh is arrested by a relatively flat or slightly rising plateau, after which a gradual decrease sets in. This same pattern prevails for the 60° turn for

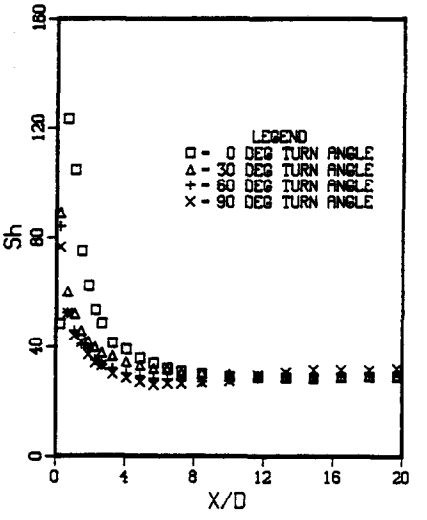

FIG. 9. Sherwood number distributions in the mass transfer section downstream of a bend fed through a sharp-edged inlet, $Re \cong 5380$.

$Re = 24\,500$. Other distributions exhibit rolls. These features reflect the transformation of the complex, three-dimensional velocity field exiting the bend into the simple pipe-flow velocity profile.

With regard to the effect of the bend on the magnitude of the Sherwood number, there appears to be a trend with the Reynolds number. For the lower Reynolds numbers (5450, 9090), the presence of the bend generally tends to reduce the Sherwood number relative to the no-bend case. On the other hand, for $Re = 24\,500$ and greater, the with-bend Sh are larger than those in the absence of the bend. For $Re = 15\,800$, the with-bend and no-bend results are intermingled.

For $Re = 15\,800$, the Sherwood numbers for the 30° turn are higher than the others in a significant portion of the entrance region. The top spot is shared by the 30 and 60° data for $Re = 24\,500$, whereas for the higher Reynolds numbers the 60° data are highest. Study of the relative positioning of the data for the various turning angles suggests that at still higher Reynolds numbers, beyond those investigated here, the Sherwood numbers for the 90° turn will emerge as the largest.

The extent of the mass transfer section that is affected by the presence of the bend is also dependent on the Reynolds number. For the lowest Reynolds number (5450), due to the laminarization and subsequent transition, bend effects extend to $X/D = 20$. The affected region is confined to about $X/D = 10$ for $Re = 9090$ and 15 800. Thereafter, as the Reynolds number increases, the affected region extends out to about $X/D \cong 15$.

Sharp-edged bend inlet

The Sherwood number distributions in the post-bend mass transfer section are presented in Figs. 9–13 for the case of a bend fed from a large upstream

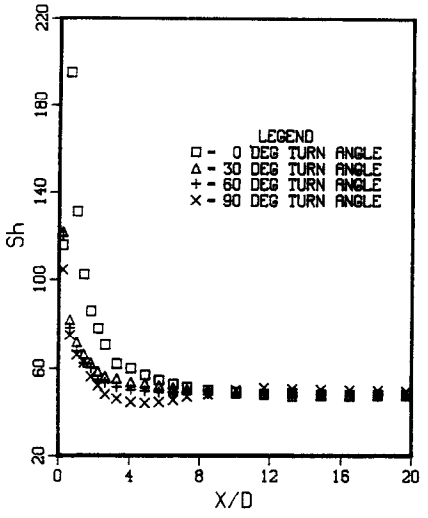

FIG. 10. Sherwood number distributions in the mass transfer section downstream of a bend fed through a sharp-edged inlet, $Re \cong 9080$.

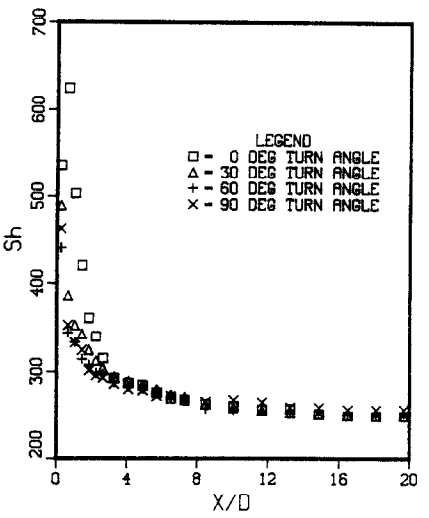

FIG. 12. Sherwood number distributions in the mass transfer section downstream of a bend fed through a sharp-edged inlet, $Re \cong 61\,400$.

plenum through a sharp-edged inlet. The format of these figures is identical to that of Figs. 3–8. Each of the figures is for a specific Reynolds number, and the data in each figure are parameterized by the turn angle of the bend. The Reynolds number for each figure is an average over the four turn angles. The greatest spread about the average occurs in Fig. 9, where the Reynolds number for the 0° case is 5140, while the 30, 60, and 90° bends group around an average Re of 5470. This spread does not affect the qualitative comparison of the with-bend and no-bend results. The Reynolds number spreads in the other figures are substantially smaller.

For the case of the sharp-edged bend inlet, an all-encompassing generalization can be made about the effect of the presence of the bend, namely, that the Sherwood numbers are reduced by the presence of the bend. Furthermore, for the most part, the data for each Reynolds number are arranged in a regular order with turn angle, decreasing as the turn angle increases from 0 to 90°. The regularity of the results enabled the omission of one of the Reynolds numbers that had been included for the case of the tube-fed inlet. Also noteworthy is the relatively short portion of the mass transfer section that is affected by the bend. The affected region extends to $X/D = 8$ for $Re = 5380$ and 9080, but only to $X/D = 4$–5 for higher Reynolds numbers.

The bend-related decrease in Sherwood numbers downstream of the bend can be made plausible by considering the flow pattern associated with a sharp-edged inlet. Such an inlet causes separation of the

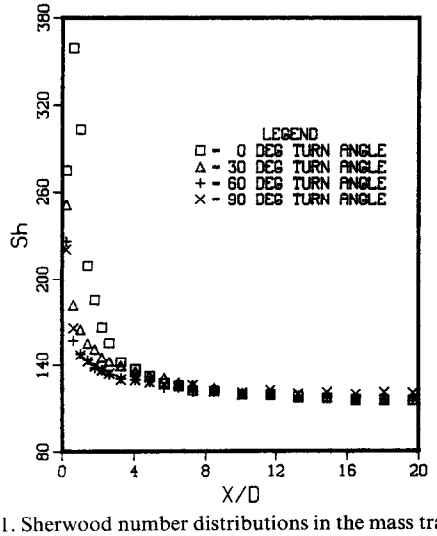

FIG. 11. Sherwood number distributions in the mass transfer section downstream of a bend fed through a sharp-edged inlet, $Re \cong 24\,700$.

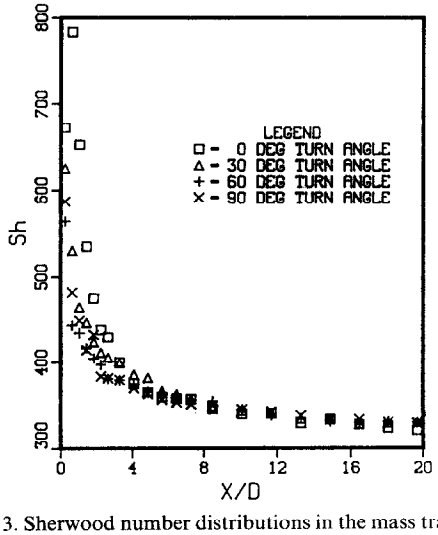

FIG. 13. Sherwood number distributions in the mass transfer section downstream of a bend fed through a sharp-edged inlet, $Re \cong 84\,300$.

flow, followed by reattachment and redevelopment. This sequence of events at the inlet of a conventional (straight) mass or heat transfer section gives rise to a Sherwood or Nusselt number distribution characterized in succession by an initial sharp rise, the attainment of a maximum, and a smooth, monotonic decrease to the fully developed state. This pattern is in evidence for the no-bend case (0° turn angle) in Figs. 9–13. Of particular significance is that Sherwood or Nusselt numbers downstream of a sharp-edged inlet are considerably larger than those for a conventional entrance region where the velocity profile is axially unchanging and fully developed (e.g. Figs. 2 and 3 of ref. [9]).

With the bend in place upstream of the mass transfer section, the processes of flow separation and reattachment are completed within the bend. As a consequence, the mass transfer section does not benefit from the enhancement associated with these processes. In particular, the initial sharp rise and the maximum are absent from the Sherwood number distributions for the 30, 60, and 90° bends. Rather, these distributions exhibit an immediate decrease. It is the loss of the separation-related enhancement which causes the Sherwood number distributions for the with-bend case to fall below that for the no-bend case. The greater the angle of turn, the greater is the post-reattachment redevelopment, which occurs in the bend, and the lower the Sherwood numbers in the mass transfer section.

The processes of bend-induced laminarization and subsequent transition to turbulence are manifested by the undershoot of the Sherwood number distributions for the 60 and 90° cases in Fig. 9 ($Re = 5380$) and for the 90° case in Fig. 10 ($Re = 9080$). Relative to the respective fully developed values, these undershoots are about 15% for $Re = 5380$ and about 10% for $Re = 9080$.

As a final note with respect to Figs. 9–13, it may be verified that the percentage spread of the data with turn angle at a given Reynolds number diminishes as the Reynolds number increases. This behavior is somewhat obscured by the different ordinate scales used for the respective figures.

Comparisons for the two bend inlet configurations

Thus far, the results corresponding to the two investigated bend inlet configurations have been reported separately, in Figs. 3–8 for the tube-fed bend inlet and in Figs. 9–13 for the sharp-edged bend inlet, respectively. Now, representative results for the two configurations will be brought together and compared, and Figs. 14–17 have been prepared for this purpose. The successive figures correspond respectively to turn angles of 0, 30, 60, and 90°. Each figure conveys results for several representative Reynolds numbers, and for each Reynolds number, data are presented for the tube-fed bend inlet (open symbols) and the sharp-edged bend inlet (black symbols).

The Reynolds numbers for the results exhibited in each figure are listed in the legend in the top right-hand corner of that figure. Note that the circle and square symbols are used repeatedly because of their availability in both open and black form in the graphics package. No ambiguity will result from the multiple use of these symbols when it is realized that the data in each figure are naturally arranged in ascending order with increasing Reynolds number.

An overview of Figs. 14–17 indicates that the most significant differences between the Sherwood number results for the two inlet configurations occur for the

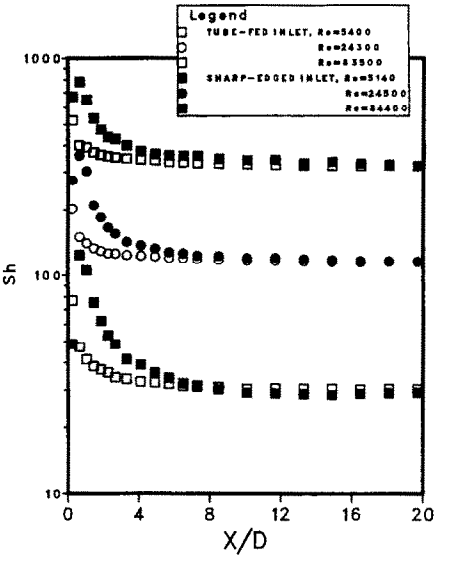

FIG. 14. Comparisons of Sherwood number distributions corresponding to bends with tube-fed and sharp-edged inlets, turn angle of 0°.

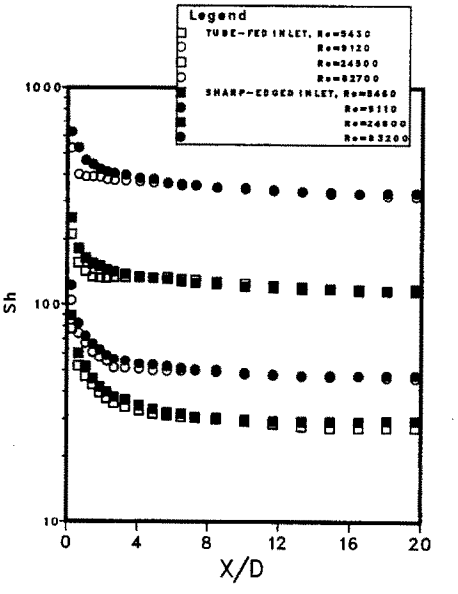

FIG. 15. Comparisons of Sherwood number distributions corresponding to bends with tube-fed and sharp-edged inlets, turn angle of 30°.

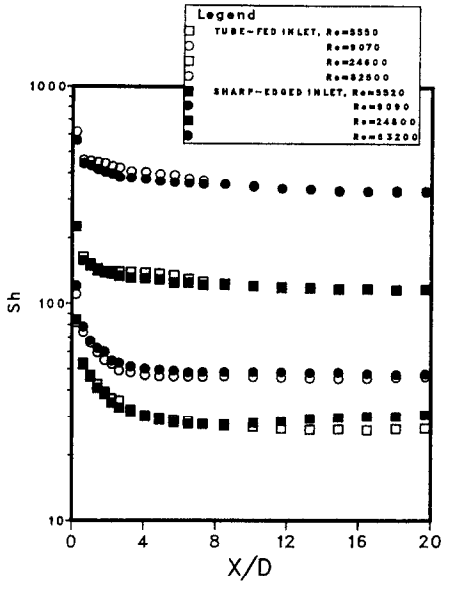

FIG. 16. Comparisons of Sherwood number distributions corresponding to bends with tube-fed and sharp-edged inlets, turn angle of 60°.

no-bend case (0° turn angle), with substantially smaller differences when a bend is in place. For the no-bend case, the differences between the results for the two inlets are due to the presence or absence of flow separation in the initial portion of the mass transfer section. With separation present (sharp-edged inlet), the entrance region Sherwood numbers are considerably higher than those without separation (tube-fed inlet), as discussed earlier. Also, the shapes of the Sherwood number distributions are characteristically different, as per the earlier discussion. The

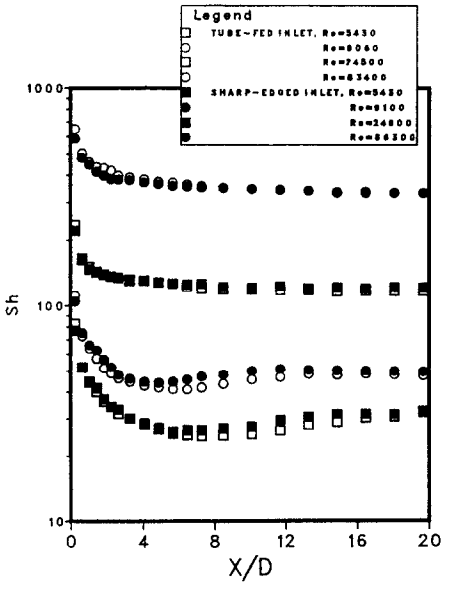

FIG. 17. Comparisons of Sherwood number distributions corresponding to bends with tube-fed and sharp-edged inlets, turn angle of 90°.

paired distributions for the no-bend case have more or less merged at $X/D = 6$–8.

The presence of the bend tends to screen the mass transfer section from the specifics of the flow configuration at the bend inlet. The greater the bend turn angle, the more effective should be the screening. Thus, the results for the 30° bend are somewhat more sensitive to the bend inlet configuration than are the results for larger turn angles. This is especially true for the higher Reynolds numbers for the 30° case; but even there the paired distributions have merged by $X/D = 4$. Whenever differences occur for the 30° case, the values of Sh corresponding to the sharp-edged inlet are greater, which is a carryover from the no-bend case.

For the 60° case, aside from what may be an anomaly at large X/D for $Re \cong 5500$, the deviations are generally small. The values of Sh for the tube-fed inlet are slightly greater than those for the sharp-edged inlet at higher Reynolds numbers, with a reversed relationship at lower Reynolds numbers. For the 90° case, the deviations are confined to the laminarization and transition regimes for lower Reynolds numbers.

CONCLUDING REMARKS

The experiments performed here have provided definitive information on the effect of a bend on the mass (heat) transfer characteristics in a straight tube situated downstream of the bend. Three parameters were varied during the course of the experiments. One of these was the Reynolds number, which encompassed the range from about 5000 to 85000. The second parameter was the turn angle of the bend, the values of which were 0, 30, 60, and 90°. The 0° turn angle corresponds to no bend in place, and this case was used as a baseline against which were compared the results obtained in the presence of the bend.

The third parameter was the hydrodynamic inlet configuration of the bend. In one case (tube-fed bend), the bend inlet was fed by a hydrodynamically developed tube flow. In a second case (sharp-edged inlet), the bend was fed from a large upstream plenum through a sharp-edged inlet. Air was the working fluid, and mass transfer measurements were made via the naphthalene sublimation technique.

It was found that the presence of a bend with a sharp-edged inlet gave rise to Sherwood numbers in the downstream tube which were lower than those for the no-bend case (i.e. those for a tube with a sharp-edged inlet). However, in the case of the tube-fed bend, the comparison of the with-bend and no-bend results is not as clear cut. For the lower Reynolds numbers, the presence of the bend generally tended to reduce the Sherwood numbers in the downstream tube relative to those without the bend (i.e. those for a tube fed with a hydrodynamically developed flow). On the other hand, for the larger Reynolds numbers, the with-bend Sherwood numbers were greater than the no-bend values.

The sensitivity of the tube Sherwood numbers to the fluid inlet configuration was greatest for the no-bend case. The presence of the bend tended to screen the tube from the specifics of the flow configuration at the bend inlet.

At the lower investigated Reynolds numbers ($\sim$5500 and 9000) and the largest bend turn angle (90°), there was clear evidence of laminarization of the flow in the initial portion of the mass transfer tube. At greater downstream distances, the laminarized (or partially laminarized) flow underwent a transition to turbulence. The laminarization was evidenced by an undershoot of the Sherwood number distribution relative to the fully developed value. The undershoot was observed for both of the investigated flow inlet configurations for the aforementioned Reynolds numbers and turn angle. It was also observed for a turn angle of 60° for $Re \sim 5500$ and the sharp-edged inlet configuration. The laminarization of the flow in the tube is a continuation of the laminarization process begun in the bend upstream of the tube.

REFERENCES

1. E. M. Sparrow and G. M. Chrysler, Turbulent flow and heat transfer in bends of circular cross section: I—heat transfer experiments, *J. Heat Transfer* **108,** 40–47 (1986).
2. G. M. Chrysler and E. M. Sparrow, Turbulent flow and heat transfer in bends of circular cross section: II—pressure distribution experiments, *J. Heat Transfer* **108,** 212–216 (1986).
3. G. I. Taylor, The criterion for turbulence in curved pipes, *Proc. R. Soc. London* **A124,** 243–249 (1929).
4. R. Narasimha and K. R. Sreenivasan, Relaminarization of fluid flows, *Adv. Appl. Mech.* **19,** 221–309 (1979).
5. S. A. Berger, L. Talbot and L. S. Yao, Flow in curved pipes, *Ann. Rev. Fluid Mech.* **15,** 461–512 (1983).
6. M. M. Ohadi, Turbulent swirl-affected heat transfer and pressure drop characteristics in a straight tube situated downstream of a bend, Ph.D. Thesis, Department of Mechanical Engineering, University of Minnesota, Minneapolis, Minnesota (1986).
7. M. Molki and E. M. Sparrow, In-tube heat transfer for skewed inlet flow caused by competition among tubes fed by the same plenum, *J. Heat Transfer* **105,** 870–877 (1983).
8. H. H. Sogin, Sublimation from disks to air streams flowing normal to their surfaces, *Trans. Am. Soc. Mech. Engrs* **80,** 61–71 (1958).
9. E. M. Sparrow and M. M. Ohadi, Comparison of turbulent thermal entrance regions for pipe flows with developed velocity and velocity developing from a sharp-edged inlet, *J. Heat Transfer* **109,** 1028–1030 (1987).
10. E. M. Sparrow and M. M. Ohadi, Numerical and experimental studies of turbulent heat transfer in a tube, *Numer. Heat Transfer* **11,** 461–476 (1987).

TRANSFERT THERMIQUE DANS UN TUBE DROIT SITUE EN AVAL D'UN COUDE

Résumé—La variation axiale du coefficient local de transfert thermique dans un tube droit situé en aval d'un coude est mesurée par une technique de transfert de masse pour les valeurs paramétriques du nombre de Reynolds (5000–85 000), angle de cintrage du coude (0, 30, 60 et 90°), et condition de l'écoulement à l'entrée du coude. Pour une condition d'écoulement, l'entrée du coude est un écoulement hydrodynamiquement établi. Dans un second cas, le coude est alimenté à partir d'une grande chambre de tranquillisation à travers une entrée à bord mince. Le nombre de Schmidt pour le transfert de masse est 2,5 (sublimation du naphtalène dans l'air). Il est trouvé que le second cas provoque une décroissance des coefficients de transfert de masse (de chaleur) dans le tube en aval, par comparaison avec ceux du cas sans coude. D'un autre côté, le premier cas tend à diminuer les coefficients dans le tube en aval pour les bas nombres de Reynolds et à les augmenter pour les grands nombres. A la fois pour les deux configurations d'entrée, il y a l'évidence d'une laminarisation de l'écoulement avec les plus faibles nombres de Reynolds et les plus grands angles de cintrage.

WÄRMEÜBERGANG IN EINEM GERADEN ROHR HINTER EINER KRÜMMUNG

Zusammenfassung—Die axiale Verteilung des örtlichen Wärmeübergangs-Koeffizienten in einem geraden Rohr hinter einer Krümmung wurde mit Hilfe der Sublimationstechnik für verschiedene Werte der Reynolds-Zahl (5000–85 000), des Krümmungswinkels (0, 30, 60 und 90°) und der Strömungsbedingungen am Krümmungseintritt bestimmt. In einem Fall war die Strömung am Krümmungseintritt hydrodynamisch ausgebildet; im zweiten Fall erfolgt die Zuströmung aus einem großen, stromaufwärtsgelegenen Plenum mit scharfkantigem Einlauf. Die Schmidtzahl für den Stoffübergang ist 2,5 (Naphtalinsublimation in Luft). Es zeigte sich, daß eine Krümmung, die über einen scharfkantigen Einlauf aus einem großen Plenum versorgt wird (Fall 2), eine Abnahme des Stoff- (Wärme-) Übergangs-Koeffizienten hervorruft im Vergleich zum Fall ohne Krümmer. Auf der anderen Seite nehmen hinter einer Krümmung, die von einer ausgebildeten Strömung versorgt wird, die Koeffizienten bei kleinerer Reynolds-Zahl ab, bei großer Reynolds-Zahl zu. Für beide Einlaufkonfigurationen gibt es klare Hinweise für eine Laminarisierung der Strömung bei kleinen Reynolds-Zahlen und großen Krümmungswinkeln.

ТЕПЛОПЕРЕНОС НА ПРЯМОМ, РАСПОЛОЖЕННОМ ЗА ИЗГИБОМ УЧАСТКЕ ТРУБЫ

Аннотация—Аксиальное изменение локального коэффициента теплопереноса на прямом участке трубы, находящемся вниз по течению за изгибом, исследуется с использованием техники переноса масы в диапазоне значений числа Рейнольдса от 5000 до 85 000 при углах изгиба 0, 30, 60 и 90° и для различных условий течения на входе в изгиб. В одном случае на входе в изгиб профиль скорости потока является развитым. В другом — поток вытекает из резервуара под давлением через отверстие с острыми краями. Число Шмидта для массопереноса составляет 2,5 (сублимация нафталина в воздухе). Найдено, что при истечении по второй схеме наличие изгиба приводит к уменьшению коэффициентов массо- (тепло-) переноса на участке трубы, расположенном ниже по течению, по сравнению со случаем без изгиба. При организации течения по первой схеме изгиб вызывает уменьшение этих коэффициентов в трубе, расположенной вниз по течению, при низких числах Рейнольдса и их увеличение при высоких числах Рейнольдса. В обоих случаях ламинаризация течения наблюдается при более низких числах Рейнольдса и при более высоких значениях углов изгиба.